Analytical Methods

Accepted Manuscript

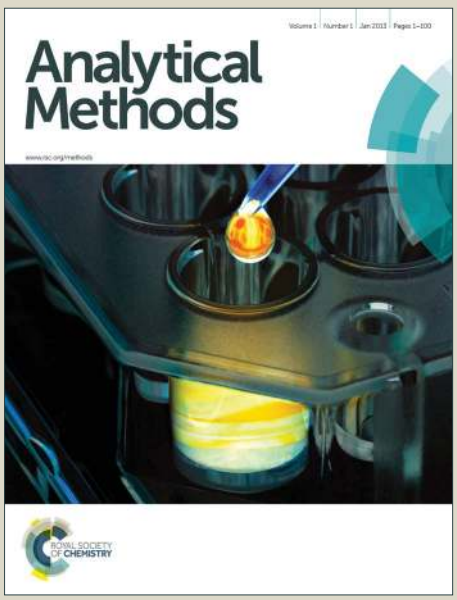

This is an *Accepted Manuscript*, which has been through the Royal Society of Chemistry peer review process and has been accepted for publication.

Accepted Manuscripts are published online shortly after acceptance, before technical editing, formatting and proof reading. Using this free service, authors can make their results available to the community, in citable form, before we publish the edited article. We will replace this *Accepted Manuscript* with the edited and formatted *Advance Article* as soon as it is available.

You can find more information about *Accepted Manuscripts* in the Information for Authors.

Please note that technical editing may introduce minor changes to the text and/or graphics, which may alter content. The journal's standard Terms & Conditions and the Ethical guidelines still apply. In no event shall the Royal Society of Chemistry be held responsible for any errors or omissions in this *Accepted Manuscript* or any consequences arising from the use of any information it contains.

ROYAL SOCIETY OF CHEMISTRY

www.rsc.org/methods

Analytical Methods

RSC Publishing

ARTICLE

Gallium telluride quantum dots bioelectrode system for human epidermal growth factor receptor-2 (Her2/neu) oncogene signalling

Cite this: DOI: 10.1039/x0xx00000x

Received 00th April 2015,
Accepted 00th Month 2015

DOI: 10.1039/x0xx00000x

www.rsc.org/

Xolile Fuku[a], Baljit Singh[b], Rachel F. Ajayi[a], Abongile N. Jijana[a], Priscilla Baker[a], Eithne Dempsey[b] and Emmanuel Iwuoha[a*]

[a]SensorLab, Department of Chemistry, University of Western Cape, Robert Sobukwe Road, Bellville, Cape Town 7535, South Africa.
[b]Centre for Research in Electroanalytical Technologies (CREATE), Department of Science, Institute of Technology Tallaght, Dublin 24, Ireland.
[*]e-mail: eiwuoha@uwc.ac.za

Human epidermal growth factor receptor 2 (Her2/neu) is a biomarker that is overexpressed in human breast cancers. A quantum dots (QDs) based genosensor for Her2/neu oncogene was developed with gallium telluride QDs and amine-terminated probe ssDNA (NH_2-5′-AATTCCAGTGGCCATCAA-3′), that is complimentary to the DNA sequence of a section of the ERF gene of HER-2/neu (i.e. 5′-GAACATGAAGGACCGGTGGGC-3′). The QDs were highly crystalline, 6 nm in size and 3.4 eV in median band-gap. The sensor sensitivity and limit of detection values were 10.0 μA ng^{-1} mL^{-1} and 0.2 pg mL^{-1} Her2/neu oncogene, respectively. Cytotoxicity studies using A549 human bronchial lung epithelial cells indicate that the genosensor can be customised for *in vivo* application.

Analytical Methods

RSC Publishing

Introduction

Breast cancer is the most common female cancer both in developed and developing countries.[1, 2] Invasion and metastasis are the root causes of cancer death[3] with the initial step being the breakdown of extracellular matrix by invading cancer cells via a concerted action of proteolytic enzymes (such as matrix metalloproteinases, MMPs), particularly the gelatinases MMP2 and MMP9.[4,5] The secretion and activity of these enzymes are partially dependent on the human epidermal growth factor receptor 2 (HER2) pathway,[6,7] which is amplified and overexpressed in breast cancer.[8] HER2 overexpression drives breast cancer cell growth by upregulating the expression of MMP2 and MMP9, resulting in accelerated degradation of type IV collagen.[9,10]

Currently, immunohistochemistry (IHC) to detect protein overexpression and gene amplification using fluorescence *in situ* hybridisation (FISH) are commonly employed approaches for assessing HER2 status in clinical specimens. IHC is prone to interfering factors, sensitivity issues, high discrepancy between laboratories, and subjective interpretation.[11-14] IHC is a semi-quantitative technique, while FISH is now considered as ''gold standard'' for HER2 determination. The latter, however is expensive, labour intensive and time-consuming, requiring specialized expertise and equipment,[11-13,15]. Moreover, gene amplification detected by FISH does not necessarily indicate protein translation and functional expression.[11,16,17] Therefore, a quantitative, accurate, cost effective and cconvenient method for HER2 protein detection is highly desirable.[11,13]

Nanoscience has become one of the most exciting areas in scientific research, with experimental developments being driven by pressing demands for new technological applications. New kinds of nano-materials which could be used in forensic science, biomedical diagnostics, electronic and sensor technologies, environmental and agri-food industries have been proposed. Due to high surface-to-volume ratio, electro-catalytic activity, biocompatibility and electron transport properties, quantum dots (QDs) are highly attractive materials for ultra-sensitive detection of biological macromolecules via bio-electronic or bio-optic transduction.[18,19] They possess unique optical and electronic properties which are capable of producing fluorescence signals that depend on size and composition.[20] and have applications which range from medicine to energy.[21,22] Compared with traditional organic fluorophores and fluorescent proteins, QDs are superior in fluorescence brightness, emission tunability and photo-bleaching resistance.[23] In addition, QDs have broad absorptions with narrow emission spectra, and different colors. They can be excited simultaneously by a single-light source, with minimal spectral overlapping.[24, 25] These unique optical properties make QDs ideal candidates for multi-color imaging of molecules in order to investigate the dynamic cellular processes of cancer progression, such as continual cell migration, invasion and metastasis.[3, 26–28] However, the clinical application of QDs-based probes *in vivo* has been limited by potential cytotoxicity effects,[27–29] and clinical application should firstly involve *in vitro* studies,[30] especially in molecular pathology.[31] The advances of QDs-based probes for breast cancer have demonstrated a promising preclinical application in recent studies.[30, 32–37]

The focus of this study is demonstration of HER2/neu complimentary DNA detection using a Ga_2Te_3 modified electrode surface. This approach opens up development of DNA-based genosensors for the detection of transgenes or biomarkers for breast cancer.

Experimental Procedures

Reagents and materials

Gallium metal (99.99%), tellurium powder (99.99%), sodium borohydride (99.99%), 3-Mercaptopropionic acid (MPA, 99.0%), acetone, 1-ethyl-3-(3-dimethylaminopropyl) carbodiimide hydrochloride (EDC), N-hydroxysuccinimide (NHS), pH 8.00 ± 0.1, perchloric acid ($HClO_4$), sodium hydroxide (99.9%) and hydrochloric acid (75%) were all purchased from Sigma-Aldrich. 18-21 base oligonucleotide DNA sequences were purchased from Inqaba Biotechnical Industries (Pty) Ltd., Hatfield, South Africa and Eurogentec S.A, Rue du Bois Saint Jean, 5, 4102 Seraing, Dublin). Base sequences: *Amine terminated DNA with the sequence NH_2-5'-AAT TCC AGT GGC CAT CAA-3', was used as the probe ssDNA. Target DNA (complementary): 5'-GAA CAT GAA GGA CCG GTG GGC-3', - a section of ERF gene of HER-2/neu. Non complementary: 5'-CAT AGT TGC AGC TGC CAC TG-3'. 3-base mismatch: 5'-GAT CAT GAA GCA CCG GAG GG-3'.* The oligonucleotide DNA stock solutions were prepared using phosphate buffer and stored in a freezer at (-20 °C). Phosphate buffer solution (PBS), 0.1 M, pH 7.4 was prepared from anhydrous potassium hydrogen phosphate (K_2HPO_4) and potassium dihydrogen phosphate (KH_2PO_4). Deionized water (18.2 MΩ) purified by a Millipore system (Synergy) was used for aqueous solution preparations.

Synthesis of Ga_2Te_3 quantum dots

3.87 g of Ga metal and 2 mL of concentrated $HClO_4$ were added to a round bottomed flask and refluxed under constant stirring for 8 h at 120 °C, after which a white precipitate of $Ga(ClO_4)_3.6H_2O$ was formed. 380 mg of the Gallium salt was then dissolved in 20 mL of distilled water followed by addition of 138.9 µL of capping agent MPA (concentrated solution : 4.06 µM). The pH of the solution was adjusted to 12 (using 1.0 M NaOH) and saturated with N_2 for 1 h.

Te^{2-} was prepared by mixing 32 mg of Te powder with 16.0 mg sodium borohydride dissolved in 20 mL distilled water, under an inert atmosphere (N_2). The mixture was then stirred continuously (8 h) at room temperature under nitrogen saturation, after which a dark purple solution was formed. Freshly prepared Te^{2-} was added dropwise into the nitrogen saturated $Ga(ClO_4)_3$/MPA solution followed by reflux for 4 h resulting in a yellow solution (Ga_2Te_3 quantum dots in solution).

For X-ray diffraction (XRD) analysis, the solution was cooled in an ice bath, following a 4 h reflux (100 °C) and precipitated by adding acetone (35 mL), drop-wise to the reaction mixture under continuous stirring. The precipitate was collected via centrifugation (10 min, 14,000 rpm) and the materials washed with water several times in order to remove free ions, using a combination of sonication and centrifugation. 70% yield of the powdered quantum dots (Ga_2Te_3) was realised and re-dispersion was possible in 0.2 M phosphate buffer (pH 7.4) when required.

Preparation of Ga_2Te_3-MPA/Au and Ga_2Te_3-MPA/GCE electrodes.

Analytical Methods ARTICLE

Gold disk electrode (Au) and glassy carbon electrode (GCE) were thoroughly cleaned by polishing using 1.00, 0.30 and 0.05 μm alumina powders and rinsing with de-ionized water. This was followed by sonication in de-ionised water for 5 min. The electrodes (Au and GCE) were drop-coated with MPA capped Ga_2Te_3 QDs solution, dried at 35 °C for 1 h, followed by gentle washing with de-ionised water to remove any loose material. The electrodes are labelled as Ga_2Te_3-MPA/Au and Ga_2Te_3-MPA/GCE. Phosphate buffer solution (0.2 M, pH 7.4) was used as electrolyte for electrochemical measurements.

DNA genosensor fabrication (dsDNA/Ga_2Te_3-MPA/Au)

The QDs modified gold electrode (Ga_2Te_3-MPA/Au) was activated via EDC-NHS steps (Scheme I) prior to ssDNA attachment. The hybridisation step was performed by immersing the probe-modified gold electrode in different concentrations 0.1 nM to 8 nM of the target DNA (complimentary) for 5 min. The as prepared electrode is labelled as dsDNA/Ga_2Te_3-MPA/Au. A CV of the hybridised electrode was recorded following the incubation step. The same protocol was applied for hybridisation reactions of the probe-modified electrode with, *1*-base mismatch sequence, *3*-base mismatch and non-complimentary DNA.

Instrumentation and electrochemical measurements

The surface morphology, size and distribution of the synthesised Ga_2Te_3 quantum dots was scrutinised using transmission electron microscope (TEM, JEOL 2011) in order to determine particle size, shape, and distribution and crystallinity. The TEM was operated at 200 kV using a LaB6 filament equipped with a Gatan multiscan camera 794 and the sample was dropcast onto Cu grids. Elemental analysis was enabled using EDX/EDS and X-ray diffraction (XRD) performed using a Rigaku D/MAX-PC 2500 X-ray diffractometer with a CuK_α (λ = 1.54 Å) radiation source operating at 40 kV and 200 mA. Fourier Transform Infrared Spectroscopy (FTIR) experiments were performed on a Perkin Elmer spectrometer (Spectrum 100), Fluorescence experiments were performed on (Type FL3- 2IHR) and UV/Vis absorption spectroscopy was performed using BioTek Synergy H1-Hybrid detector.

Electrochemical experiments {cyclic voltammetry (CV) and electrochemical impedance spectroscopy (EIS)} were performed using a CH Instruments Bioanalytical System 660 (Model No: 100B). A three-electrode electrochemical cell comprising a platinum counter electrode, Ag/AgCl reference electrode, a glassy carbon (GCE, 0.0707 cm^2) or gold (Au, 0.02 cm^2) working electrode and 0.1 M PBS (pH 7.4) as electrolyte, were used in all electrochemical experiments.

Scheme I.

Results and Discussion

Surface morphological and structural characterisation

The surface morphology, and particle size of the synthesised Ga_2Te_3 quantum dots were characterised using TEM, HR-TEM and STEM (Fig. 1 (a-f)) and provide evidence of good dispersion, indicating that the synthetic route was successful in avoiding agglomeration. Fig. 1 (a, b, and f) shows the TEM and HR-TEM images of the Ga_2Te_3 QDs. From the TEM and HRTEM data, the average diameter (n = 10) of the QDs was estimated to be 5 ± 0.5 nm. HRTEM images showed the uni-directional lattice fringes (d spacing = 0.2 nm), confirming the mono-crystallinity of the material. The FFT image is shown in Fig. 1 (e) and the results are in good agreement with HRTEM with regard to the mono-crystallinity of the QDs. The energy-dispersive X-ray spectroscopy (EDS, Fig. 1g) analysis further confirms the presence of Ga and Te in Ga_2Te_3 QDs sample which are the main components of the material. Copper was observed in the EDS spectrum as a result of the sample preparation (sample stub) used in TEM/EDS analysis.

XRD analysis was employed for the structural and size verification of the Ga_2Te_3. XRD analysis (Fig. 2A) shows the diffraction pattern with peaks positions corresponding to crystal planes (111), (200), (220), (311), (222), (400), (420) and (333).[38-39] From a careful analysis of the peak positions, lattice parameters and in accordance with the literature,[38-40] XRD patterns of the nanodots were indexed/associated to the cubic phase (zinc blende) structure for Ga_2Te_3 with lattice constant, a = 5.89Å. In the XRD patterns, the (111) plane was found to be very clear and abundant which indicates preferential growth of the crystallites. The average size was calculated using the Scherrer equation:[41]

$$d = \frac{0.9\lambda}{\beta \cos\theta} \quad \text{.....(1)}$$

where d is the crystallite size, λ is the wavelength of X-ray used (1.5418Å), β is the full width at half maximum and θ is Bragg's angle of reflection. The average particle size calculated from equation (1) was 6 nm, which is in agreement with the average size obtained from the HRTEM analysis. The peak at 57.02 degrees could be assigned to (321/2), corresponding to a chalcopyrite structure, indicating the existence of chalcopyrite-type orderings in the Ga_2Te_3 crystals.[38] Some additional peaks (Fig. 2A) were observed in the diffraction pattern which could be due to either different Te species or the existence of chalcopyrite-type orderings, and this requires further investigation.

Surface capping and functionalisation of quantum dots was intended to: stabilise the quantum dots, lower or even eliminate toxicity, prevent agglomeration and aid solubilisation. Here MPA (3-mercaptopropionic acid) acted as capping agent and it was expected that the thiol group (-SH) of the MPA would associate with the hydrophobic surface of the quantum dots[42] while the carboxylic acid group (-COOH) extends into solution to make the quantum dots more hydrophilic. Fig. 2B contains the FTIR spectrum of MPA which has vibrational stretches at 3000, 2500, 2000 and 1500 cm^{-1} due to OH, -SH, C=O and C-H, respectively. Compared to the control (MPA alone, Fig 2B(a)), the intensity of -SH stretching in the quantum dots sample (Ga_2Te_3-MPA, Fig. 2B(b)) decreased with a slight shift in wavenumbers, whilst the uncapped QDs (Ga_2Te_3, Fig. 2B(b)) showed no vibrational stretches as expected, indicating that the quantum dots (Fig. 2B(c)) were sufficiently capped with MPA.

Fig 1.

UV/Vis and fluorescence studies (Fig. 3) were carried out in order to investigate the absorption, emission and excitation wavelength of the quantum dots. The λ_{max} of MPA-Ga_2Te_3 was observed at 238 nm and that of MPA alone was observed at 298 nm, (Fig. 3(a)). The behaviour suggests that the absorption of a photon at this wavelength by MPA-Ga_2Te_3 QDs caused electronic transition from the valence band to the conduction band, thereby leaving an electron-hole pair (exciton). Electrons in the valence band are tightly coupled with their respective nuclei, whereas electrons in the conduction band are slightly separated from their nuclei, thereby allowing free electronic motion within the solid.

Fig. 2 (A) and (B)

The effect of the refluxing (during QDs synthesis) time (for 2-16 h, at 100 °C) was also monitored and the results are shown in Fig. 3a for absorption peaks at 238 nm (2 h), 241 nm (8 h) and 340 nm (16 h). This red shift over longer refluxing period indicate size increment and decrease in the band gap energies. This increment in size is due to quantum confinement effects, which may be observed when the size is sufficiently small - the energy level spacing of the nanocrystal exceeds a K_BT (K_B is Boltzmann's constant and T is temperature) value of 1.380648 $\times 10^{-23}$ J K^{-1}.[43] This effect allows the tuning of the energy-band gap with respect to size of quantum dots.

Fluorescence analysis (Fig. 3(b-c)) of Ga_2Te_3-MPA produced emission at 310 nm and excitation at 226 nm, while MPA alone was had corresponding values at 280 nm and 334 nm. The Ga_2Te_3 QDs was found to be blue shifted (by 50 nm) and the shift in wavelength was associated with Stokes shift. The energy of the emitted (310 nm) and excited (226 nm) species and the band gap energy (E_g) from the fluorescence and UV-visible analysis were calculated using the following equation:

$$E_g = \frac{hc}{\lambda} \quad \text{..... (2)}$$

where E_g is the band gap energy, h is the Planck constant (6.626 × 10^{-34} J s or 4.136 × 10^{-15} eV s), c is the speed of light = 3.0 × 10^8 cm s^{-1}, λ is the wavelength (430 × 10^{-9} m). The energy of the emitted electron was calculated to be 4.62 × 10^{-22} J for excitation and 5.37 × 10^{-22} J for the absorption. The band gap of the material was calculated to be 3.3 eV and 3.5 eV from fluorescence and UV/visible data, respectively. These values were found to be comparable and are in good agreement with the literature values.[38-41, 44,45,46-57] The band gap value suggests that the material is electrically conductive (i.e. it is a semiconductor).

Fig 3 (a), (b and c)

Electrochemical characterisation

Redox properties Ga_2Te_3-MPA QDs immobilized on GCEs were investigated prior to DNA sensing. Fig. 4A shows the CVs of the bare GCE; and MPA-, Ga_2Te_3- and (Ga_2Te_3-MPA)-modified GCEs. From the comparison of MPA-capped vs. uncapped QDs samples (Fig. 4A (c and e)), a shift in peak potential (for Te oxidation process at E_p = 270 mV) as well as significant increment in anodic and cathodic current (E_p = -700 mV for Ga^{3+} reduction wave) were observed, which may be attributed to the particle size effect. The capping agent may also have a co-catalytic effect, which is evident by an increase in the peak current of the capped (Ga_2Te_3-MPA/GCE) compared to the uncapped (Ga_2Te_3/GCE) QDs. For comparison cyclic voltammetry of ssDNA/GCE in phosphate buffer solution was also recorded (Fig. 4B). GCE was chosen specifically for this purpose due to the occurrence of gold oxidation and reduction peak currents which might interfere with the ssDNA peak currents.

Fig. 4C contains the cyclic voltammograms (CVs) of (a) Te/GCE, (b) Ga_2Te_3-MPA/GCE, (c) ssDNA/ Ga_2Te_3-MPA/GCE and (d) bare GCE; in phosphate buffer solution. Ga_2Te_3-MPA/GCE gave an anodic peak current at 350 mV, which shifted to 500 mV, upon the introduction of ssDNA. The ssDNA oxidation (Fig. 4B) was also observed at around this potential (400 mV) as well as 850 mV, and was associated with the guanine redox process (Fig. 4B (a and b)). Since a potential shift and a catalytic effect were observed at the peak occurring at 400 mV, it was used to study the interaction of the probe-ssDNA modified electrode with the target-ssDNA. Comparative electrochemical studies were also performed with Au electrodes. A clear reduction wave at -120 mV (peak labelled as c, Fig. 4D) was observed for the Au electrode, which is associated with the oxidation products of the QDs. The Au working electrode was, therefore, employed for further genosensor studies.

Scheme II represents the reaction mechanism for genosensor fabrication on Au electrode (which was selected due to its compatibility with the MPA capped QDs). The Au surface provides coupling sites for the amine-modified DNA attachment via the formation of amide linkages. The coupling was promoted by 1-ethyl-3-(3-dimethylaminopropyl) carbodiimide hydrochloride (EDC) and *N*-hydroxysuccinimide (NHS).

Fig 4. (A), (B), (C) and (D)

Scheme II: (A) The mechanism of the reaction of Ga_2Te_3-3MPA and probe-ssDNA with linkers (EDC/NHS). (B) The schematic diagram for the interaction of ssDNA/Ga_2Te_3-MPA/Au with target-ssDNA.

Fig 5. (A) and (B)

Fig. 5A depicts the Nyquist plots of the EIS data for experiments performed with bare Au, Ga_2Te_3-MPA/Au and ssDNA/Ga_2Te_3-MPA/Au electrodes. The aim of the EIS experiment was to investigate the behaviour of the modified and unmodified electrodes at an applied potential of 400 mV (observed from CV measurements, Fig. 4A). The R_{ct} values were calculated by fitting the EIS data to the electrical circuit diagram drawn as Fig. 4A inset. The R_{ct} values for bare Au, Ga_2Te_3-MPA/Au and ssDNA/Ga_2Te_3-MPA/Au were 11.93, 9.02 and 10.32 Ω, respectively. This indicates a more conducting surface (faster charge transport at electrode/solution interface) for Ga_2Te_3-MPA/Au, relative to both the bare Au and ssDNA/Ga_2Te_3-MPA/Au. R_{ct} represents the resistance to the charge transfer between the electrolyte and the electrode and contains information on the electron transfer kinetics of the redox probe at the electrode-electrolyte interface. The surface coverage (θ) of Ga_2Te_3-MPA/Au was 0.78 cm s^{-1} and the electron transfer rate constant (k_{et}) values for bare Au, Ga_2Te_3-MPA/Au and ssDNA/Ga_2Te_3-MPA/Au (at 400 mV) were calculated to be 1.79 × 10^{-11} s^{-1}, 2.22 × 10^{-10} s^{-1} and 1.48 × 10^{-10} s^{-1}, respectively.

The Bode plot (Fig. 5B) confirms the electrical properties of the nano-material and is in agreement with the Nyquist plot, where the modified electrode showed improved conductivity based on the phase angle of the material – 0 θ (insulator) , 20-45 θ (semiconductor) and 90 θ (conducting - pure metal). The actual phase angles for bare Au, Ga_2Te_3-MPA/Au and ssDNA/Ga_2Te_3-MPA/Au were found to be 79 θ, 71 θ and 63 θ, respectively. The Ga_2Te_3-MPA/Au is relatively more conducting due to the contributions of R_s, R_{ct} and CPE (R_s + R_{ct} + CPE) in the electrical circuit, which are more predominant than in ssDNA/Ga_2Te_3-MPA/Au which has a mixture of R_s, and R_{ct} (R_s + R_s + R_{ct}) circuit elements; meaning that the solution resistance is more predominant than charge transfer resistance. (R_s, R_{ct} and CPE are the solution resistance, charge transfer resistance and constant phase element, respectively). The total impedance, Z, data of Fig. 5B confirmed the conductive nature of the Ga_2Te_3-MPA/Au. At log F = 0, the log Z(Ga_2Te_3-MPA/Au) = 4.3, whereas log Z(bare Au) = log Z(ssDNA/Ga_2Te_3-MPA/Au) = 4.7. This means that when the electrode systems were subjected to minimal frequency effects the

Analytical Methods ARTICLE

QDs (which has additional metals in the system and without insulating oligonucleotide chains) is more conducting than the semiconducting gold electrode. There is a shift log 2 magnitude shift (increase) in frequency on changing from Ga_2Te_3-MPA/Au (1.74) electrode to ssDNA/Ga_2Te_3-MPA/Au (1.05) genosensor, due to the incorporation of the insulating probe-ssDNA in the sensor system.

Genosensor response studies

Cyclic voltammetry was used to study the binding event of the probe-ssDNA and the target-ssDNA (i.e. the complementary Her2 oncogene). Voltammograms with redox properties of gold electrode were observed with an oxidation peak potential ($I_{p,a}$) at E_p = 800 mV and a reduction peak potential ($I_{p,c}$) at E_p = 500 mV, Figure 6 A, b′, b″ and 6 C, b. Shoulders or small reduction peaks were observed at oxidation peak potential ($I_{p,a}$) of E_p = -100 mV which can be due to the products of QDs, E_p = -500 mV which was associated with redox properties of Ga^{3+} (Figure 6 A, d and 6 C, a) and at E_p = -850 mV which was associated with redox properties of Te^{2-}, Figure 6 A, e. The attenuation of the anodic peak current of ssDNA /Ga_2Te_3-MPA/Au at 400 mV (Fig. 6A (a)) due to the electrostatic interaction between the genosensor and the Her2 oncogene, was used to study the genosensing process. This interaction was made possible by the covalent attachment of the probe-ssDNA on the surface of the Au electrode. To achieve this, a probe-DNA and the surface onto which the it is to be immobilized may be modified by introducing reactive functional groups that will allow covalent coupling.[47] Several functionalities on either the electrode or the probe-ssDNA have been reported for stable anchoring of the probe on the electrode surface. Commonly used reactive functional groups include thiol, carboxyl and amino groups.[48] Covalent coupling via functionalised probe or electrode surfaces are usually accompanied by chemical activation steps.[49,50]

Fig 6. (A), (B), (C) and (D)

Table 1. Comparison of genosensor with other methods for HER2/neu oncogene determination (The original values are all converted to ng mL^{-1})

Technique	*DLR* (ng mL^{-1})	*LOD* (ng mL^{-1})	Sensitivity (μA ng^{-1} mL^{-1})
Genosensor: ssDNA/Ga_2Te_3-MPA/Au	0.03-0.55	0.0002 --	2-10
PZT/glass PEMS [29]	-	13	111
PCR [19]	28	0.06	5.5
ELISA [26]	185-46250	100	0.1
Nanoimmunoassay [52]	2-20000	1000	180
Opto-Fluidic Ring Resonator (OFRR)[53]	13-100	10	20
Biosensor: Surface Acoustic Wave (SAW)[54]	13-20	10	-

The binding-event that occurred after the introduction of 0.5 nM of Her2 oncogene in cell system containing the genosensor is presented in Fig. 6A (a). The plot showed a decrease in current as the concentration increases, which confirmed the binding of the analyte and the probe-ssDNA at the electrode interface. A shift in peak potentials (~ 50 mV) was also observed, which is characteristic of an electrode reaction involving slow electron transfer kinetics. The genosensor calibration plot is presented in Fig. 6B. It was clear from the plot that the sensor reached its point of saturation around 3 nM. The sensitivity of the genosensor was found to be 2.8×10^{-2} μA ng^{-1} mL^{-1}, the dynamic linear range (*DLR*) was calculated to be 0.5-3.0 nM and its limit of detection (*LOD*) was calculated to be 0.7 pg mL^{-1}.

Fig. 7

Square wave voltammetry (Figure 6C) showed two unresolved peaks, at 400 mV and at 800 mV. These two peaks are due to the ssDNA/Ga_2Te_3–MPA and the unreacted tellurium (Te^o). The two peaks merged into single distinctive peak after the addition of target analyte. After each addition of the target analyte, the peak current at 400 mV decreased with increasing concentration of analyte (Fig. 6C). From the calibration curve (Fig. 6D), the sensitivity and the *DLR* of the system were found to be 10 μA ng^{-1} mL^{-1} and 0.1-2.0 nM, respectively (r^2 = 0.98). The *LOD* of the genosensor from the SWV was calculated to be 0.2 pg mL^{-1}. Table 1 shows the comparison of the genosensor parameters with literature values for other methodologies for determining the HER2/neu oncogene. The genosensor's *DLR* is comparable to those reported in the literature for other methods. More importantly, the *DLR* values of the genosensor are within the physiological HER2/neu oncogene concentrations in the blood of normal (2-15 ng mL^{-1}) and breast cancer (15- 75 ng mL^{-1}) patients.[51]

Cross-reactivity (selectivity and non-specific adsorption) experiments were performed to assess whether the ssDNA/Ga_2Te_3-MPA/Au responded selectively to the complementary target. In this work, the complementary target DNA, the single-base mismatch target, the three-base mismatch target and the non-complementary sequence DNA were used to study the sequence-specificity of the sensor. The CVs of the genosensor (ssDNA/Ga_2Te_3- MPA/Au) responses for 5 nM of the different target DNA molecules are plotted in Fig. 7. The oxidation signal responded differently with different analytes. These findings indicate that some of the analytes hybridization did not occur. A decrease in signal was observed when the probe electrode was hybridised with the 3-base mismatch and non-complimentary sequence, suggesting that hybridisation occured at the electrode interface. However, there was a high decrease in signal after the probe DNA was hybridised with both the complimentary and 1-base mismatch sequences. This could be due to the fact that the target analytes and the capture probe are fully bound. These results demonstrated that the complementary target sequence could form double-stranded DNA with the probe-DNA producing a significant decrease in signal. The stability and reproducibility of the probe-modified electrode was done by keeping the electrode for 5 days in the freezer (-20 °C) and cycling the modified electrode 20 times, Fig. 8. After CV analysis, the same electrode was used after several days and the oxidation peak of the sensor at +250 mV was monitored. The peak current of the electrode initially decreased slightly but remained constant after several cycles. Statistical analyses were performed based on the stability of the sensor. The average sum of peak currents (n = 9) were calculated to be 16.98, whilst the calculated standard deviation (*SD*) and the mean values were calculated to be 0.23 and 1.69, respectively. The results suggest that the genosensor only degraded by 23%. Thus the behaviour of the modified electrode proved that the electrode can be used for number of analysis.

Fig. 8

Conclusion

Novel water soluble gallium telluride quantum dots (MPA-Ga_2Te_3) were successfully synthesised and characterised using surface, structural, electrochemical and spectroscopic techniques. UV-visible, EIS and fluorescence techniques were able to determine the conductivity of the quantum dots, and semiconductor properties of the materials were confirmed. The bifunctional amphiphilic molecule (3-mercaptopropionic acid) used as capping agents

rendered the quantum dots biocompatible, soluble and stable. Electrostatic repulsion arising from dehydrogenated carboxyl groups on the surface of the quantum dot particles kept them non-agglomerated. Retention of the capping agent on the capped-quantum dot surface was confirmed by FTIR studies, which showed characteristic bands related to C-H, C=O, -SH as well as –O-H groups. By doing comparative studies between capped QDs, uncapped QDs and MPA, the observed bands were present in MPA alone and capped QDs thus confirming the presence and attachement of MPA on the QDs. In addition, the intensity of –SH band decreased or disappeared due to the strong affinity between the metal precursor gallium (Ga) and sulphur (S). Electrochemical interrogation of the Ga_2Te_3-MPA/Au electrodes and the HER2/neu oncogene sensor (ssDNA/Ga_2Te_3-MPA/Au) were perfomed. The proposed sensor showed a sensitivity of (10.0 μA ng^{-1} mL^{-1}) and *LOD* (0.2 pg mL^{-1}) as calculated from SWV measurements. The detection limit of the genosensor was significantly lower than what is reported literature values and most importantly well below physiological limits (FDA approved) for Her2/neu detection (2-15 ng mL^{-1}). Compared to other analytes, the sensor proved to be specific to the complimentary analyte. The genosensor is very promising and have the potential of being adapted for the sensitive detection of other transgenes or biomarkers for breast cancer. This experimental success with analytical (buffer-based) samples should encourage future work with clinical samples.

Acknowledgement
We acknowledge PhD bursary from DST and MINTEK NIC for Sensors and EU funding - Marie Curie IRSES FP7 *SMARTCANCERSENS.* We also acknowledge Dr Wynette Redington and Dr. Calum Dickinson at the Materials and Surface Science Institute (MSSI), University of Limerick, Ireland for XRD and TEM analysis respectively.

Note and references

[a] SensorLab, Department of Chemistry, University of Western Cape, Robert Sobukwe Road, Bellville, Cape Town 7535, South Africa. *e-mail: eiwuoha@uwc.ac.za*
[b] Centre for Research in Electroanalytical Technologies (CREATE), Institute of Technology Tallaght, (ITT Dublin), Dublin 24, Ireland.

1 A. Jemal, R. Siegel, J. Q. Xu and E. Ward, *Journal for Clinicians* 2010, 60, 277–300.
2 C. Chen, H. S. Xia Y. P. Gong, J. Peng , C. W Peng, *Biomaterials* 2010, 31, 8818–8825.
3 W. Mahmoud, A. Sukhanova, V. Oleinikov, Y. P. Rakovich, J.F. Donegan, M. Pluot, J. H. M. Cohen and Y. Volkov and Igor Nabiev, *Proteomics* 2010, 10, 700–716.
4 J. Decock, W. Hendrickx, H. Wildiers , M. R. Christiaens , P. Neven , M. Drijkoningen and Paridaens, *Clinical and Experimental Metastasis* 2005, 22, 495–502.
5 L. Nakopoulou, I. Tsirmpa, P. Alexandrou, A. Louvrou, C. Ampela, S. Markaki and P. S. Davaris, *Breast Cancer Research Treament* 2003, 77, 145-155.
6 M. J. Duffy, P. M. McGowan and W. M. Gallagher, *The Journal of Pathology* 2008, 214, 283–293.
7 S. J. Pommier, G. G. Quan, D. Christante, P. Muller, A. E. H. Newell, S. B. Olson, B. Diggs and L. Muldoon, *Annals of Surgical Oncology* 2010, 17, 613–623.
8 H. Korkaya, A. Paulson, F. Iovino and M. S. Wicha, *Oncogene* 2008, 27, 6120–6130.
9 A. Jezierska and T. Motyl, *Medical Science Monitor* 2009, 15, RA32–RA40.
10 J. M. Pellikainen, K. M. Ropponen, V. V. Kataja, J. K Kellokoski, M. J Eskelinen and V. M Kosma, *Clinical Cancer Research* 2004, 10, 7621–7628.
11 A. C. Wolff, M. E. Hammond, J. N. Schwartz, K. L. Hagerty, D. C. Allred, R. J. Cote and M. Dowsett, *Journal of Clinical Oncology* 2007, 25, 118–145.
12 S. J. Payne, R. L. Bowen, J. L. Jones and C. A. Wells, *Histopathology* 2008, 52, 82–90.
13 C. Ginestier, E. Charafe-Jauffret, F. Penault-Llorca, J. Geneix, J. Adelaide, J. Chaffanet and M. Mozziconacci, *The Journal of Pathology* 2004, 202, 286–298.
14 C. R. Taylor and R. M. Levenson, *Histopathology* 2006, 49, 411–24.
15 H. Yaziji , L. C.Goldstein, T. S Barry, R. Werling , H. Hwang , G. K. Ellis, J. R. Gralow, R. B. Livingston, A. M. Gown , *JAMA* 2004, 291, 1972–1977.
16 C. L. Hyun, H. E. Lee, K. S. Kim, S. W. Kim, J. H. Kim, G. Choe and C. Y. Park. *The Journal of Clinical Pathology* 2008, 61, 317–321.
17 I. Vanden Bempt, M. Drijkoningen and C. De Wolf-Peeters, *Current Opinion in Oncology* 2007, 19, 552–557.
18 P. M. Ndangili, P. G. L. Baker and E. I. Iwuoha, *Journal of Electroanalytical Chemistry* 2010, 643, 77-81.
19 P. J. H. Fan and S. Ai, *Sensors Actuators B: Chemical* 2010, 149, 98-104.
20 D. H. Huang, X. H. Peng, L. Su, D. S. Wang, F. R. Khuri, D. M. Shin and Z. Chen, *Nano Research* 2010, 3, 61–68.
21 J. L. Pelley, A. S. Daar and M. A. Saner, *Toxicological Sciences* 2009, 112, 276–296.
22 U. Resch-Genger, M. Grabolle, S. Cavaliere-Jaricot, R. Nitschke and T. Nann, *Nature Methods* 2008, 5, 763–775.
23 T. Jin, D. K. Tiwari, S. Tanaka and Y. Inouye, *Molecular BioSystems* 2010, 6, 2325–2331.
24 H. Zhang, D. Yee and C. Wang, *Nanomedicine* 2008, 3, 83–91.
25 A. M. Smith and S. M. Nie, *Nature Biotechnology* 2009, 27, 732–733.
26 X. Yu, L. Chen, Y. Deng, K. Li, Q. Wang, Y. Li, S. Xiao, X. Luo, J. Liu, L. Zhou, D. W. Pang, *Journal of Fluorescence* 2007, 17, 243–247.
27 C. Chen, L. D. Chen, Z. L. Zhang and Y. Li, Chin Ger, *Journal of Clinical Oncology* 2008, 7, 179–84.
28 L. D. Chen, J. Liu, X. F. Yu, M. He, X. F. Pei, Z. Y. Tang, Q. Q. Wang, D.W. Pang and Y. Li, *Biomaterials* 2008, 29, 4170–4176.
29 R. Hardman, *Environmental Health Perspective* 2006, 114, 165–172.
30 Y. Xing, Q. Chaudry, C. Shen, K. Y. Kong, H. E. Zhau, L. W. Chung, I. A.Petros, R. M. O'Regan, M. V. Yezhelyev, I. W. Simons, M. D.Wang and S. Nie, *Nature Protocols* 2007, 2, 1152–1165.
31 L. D. True and X. Gao, *Journal of Molecular Diagnostics* 2007, 9, 7–11.
32 X. Wu, H. Liu, J. Liu, K. N. Haley, J. A. Treadway, J. P. Larson, N. Ge, F. Peale and M. P.Bruchez, *Nature Biotechnology* 2003, 21, 41–46.
33 U. Resch-Genger, M. Grabolle, S. Cavaliere-Jaricot, R. Nitschke and T. Nann, *Nature Methods* 2008, 5, 763–775.
34 E. Tholouli, E. Sweeney, E. Barrow, V. Clay, J. Hoyland and R. Byers, *The Journal Pathology* 2008, 216, 275–85.
35 M. V. Yezhelyev, A. Al-Hajj, C. Morris, A. I. Marcus, T. Liu, M. Lewis,C. Cohen, P. Zrazhevskiy and J. W. Simons, *Advanced Materials* 2007, 19, 3146–3151.
36 H. Tada, H. Higuchi, T. M. Wanatabe and N. Ohuchi, *Cancer Research* 2007, 67, 1138–1144.
37 Y. Xiao, X. Gao, G. Gannot, M. R. Emmert-Buck, S. Srivastava, P. D. Wagner, M. D. Amos and P. E.Barker, *International Journal of Cancer* 2008, 122, 2178–2186.
38 Y. Otaki, Y. Yanadori, Y. Seki, M. Tadano and S. Kashida, *Journal of Solid State Chemistry* 2009, 182, 1556-1562.
39 Y. Otaki, Y. Yanadori, Y. Seki, K. Yamamoto and S. Kashida, *Acta Materialia* 2009, 57, 1392-1398.
40 K. George, C. Groot, C. Gurnani, A.L. Hector, R. Huang, M. Jura, W. Levason,and G. Reid, *Physics Procedia* 2013, 46, 142-148.
41 U.I. Kalsoom, S. Bashir and N. Ali, *Surface and Coatings Technology* 2013, 235, 297-302.
42 W.C. Chan, and S. Nie, *Science* 1998, 281, 2016-2018
43 P.J. Mohr, B.N. Taylor and D.B. Newell (2011), "The 2010 CODATA Recommended Values of the Fundamental Physical Constants" (Web Version 6.0). Database was developed by J. Baker, M. Douma, and S. Kotochigova. Available: http://physics.nist.gov/constants. National Institute of Standards and Technology, Gaithersburg, MD 20899.
44 A. J. Bard and L. R. Faulkner, *Fundamentals and Applications of electrochemical Methods* 2nd ed., Wiley, London, 2000.
45 R. Greef and H. Aulich, *Journal of Electroanalytical Chemistry* 1968, 18, 295-285.
46 M. K. P. Zuman, *Progress in Polarography* 2nd ed., Interscience New York, 1962.
47 S. P. Pack, N. K. Kamisetty, M. Nonogawa, Kamakshaiah, C. Devarayapalli, K. Ohtani,, Y. Y. K. Yamada, TsutomuKodaki and K. Makino, *Nucleic Acids Research* 2007, 35, 1-10.
48 P. D. Tam, T. Trung, M. A. Tuan, and N. D. Chien, *Journal of Physics* 2009, 187, 1-8.

Analytical Methods

ARTICLE

49 M. Dufva, *Biomolecular Engineering* 2005, 22, 173-184.
50 J. Wang, G. Liu, R. M. Jan, and Q. Zhu, *Electrochemistry Communications* 2003, 5, 1000-1004.
51 J. A. Capobianco, W. Y. Shih, G. P. Adams and W. H. Shih, *Sensors and Actuators B: Chemical* 2011, 160, 349-356
52 S. Patris, *Talanta* 2014, 130, 164–170
53 J.T. Gohring, S.D. Paul and F. Xudon, Sensors and Actuators B 2010, 146, 226-230.
54 J.G. Friederike, R. Michael and L Kerstin, *Procedia Engineering* 2010, 5 , 914-917.
55. G.Tourillon and F.J. Garnier, *Electroanalytical Chemistry* 1988, 246, 467.
56. S. M. Bouzzine, M. Hamidi and M. Bouachrine, *The Electronic Journal of Chemistry* 2009, 1, 203-214
57. J.Roncali, *Chem.ical Reviews* 1992, 92, 711.

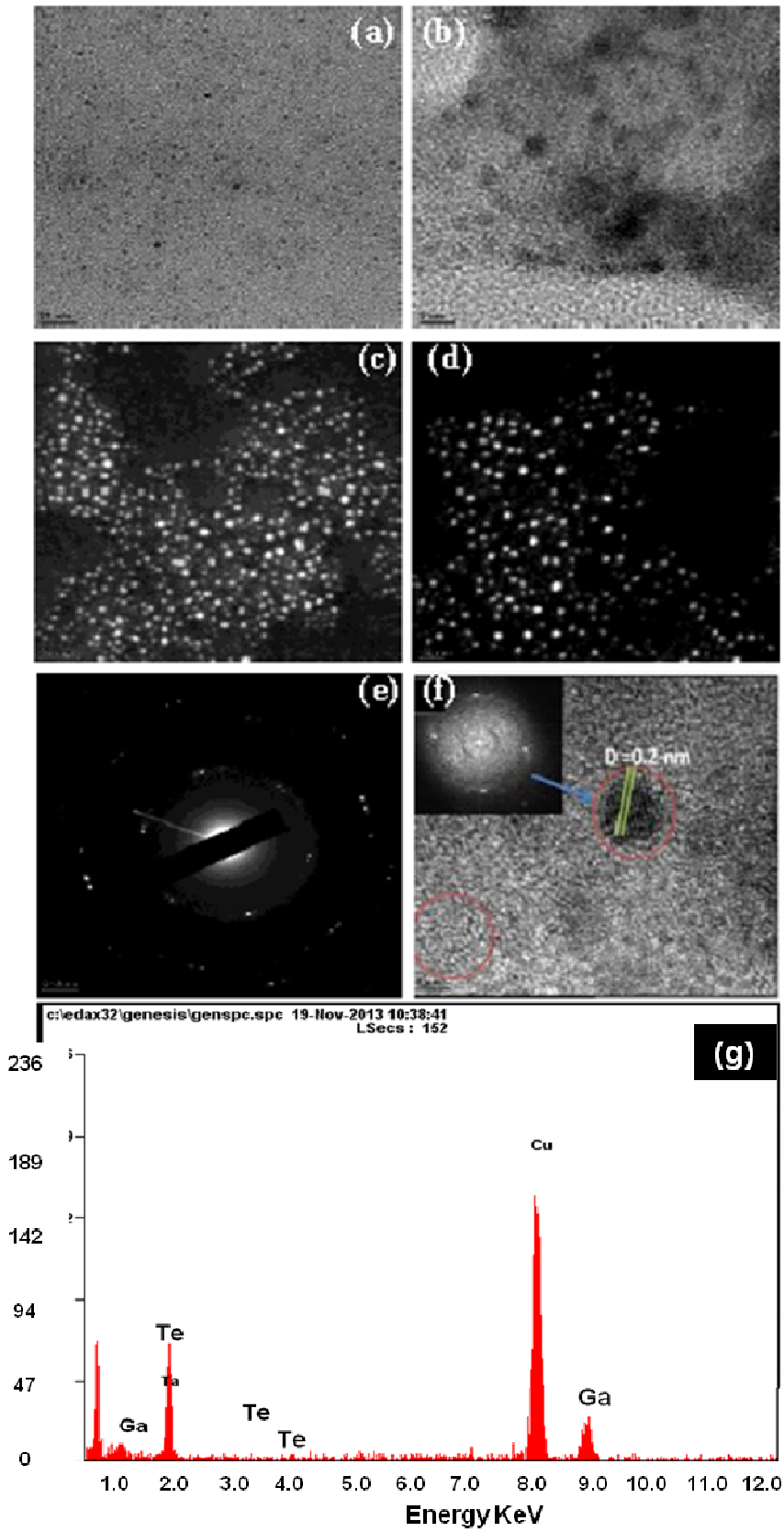

Fig 1. TEM analysis for Ga_2Te_3 quantum dots sample; (a-f) TEM images and (g) EDS spectrum for Ga_2Te_3.

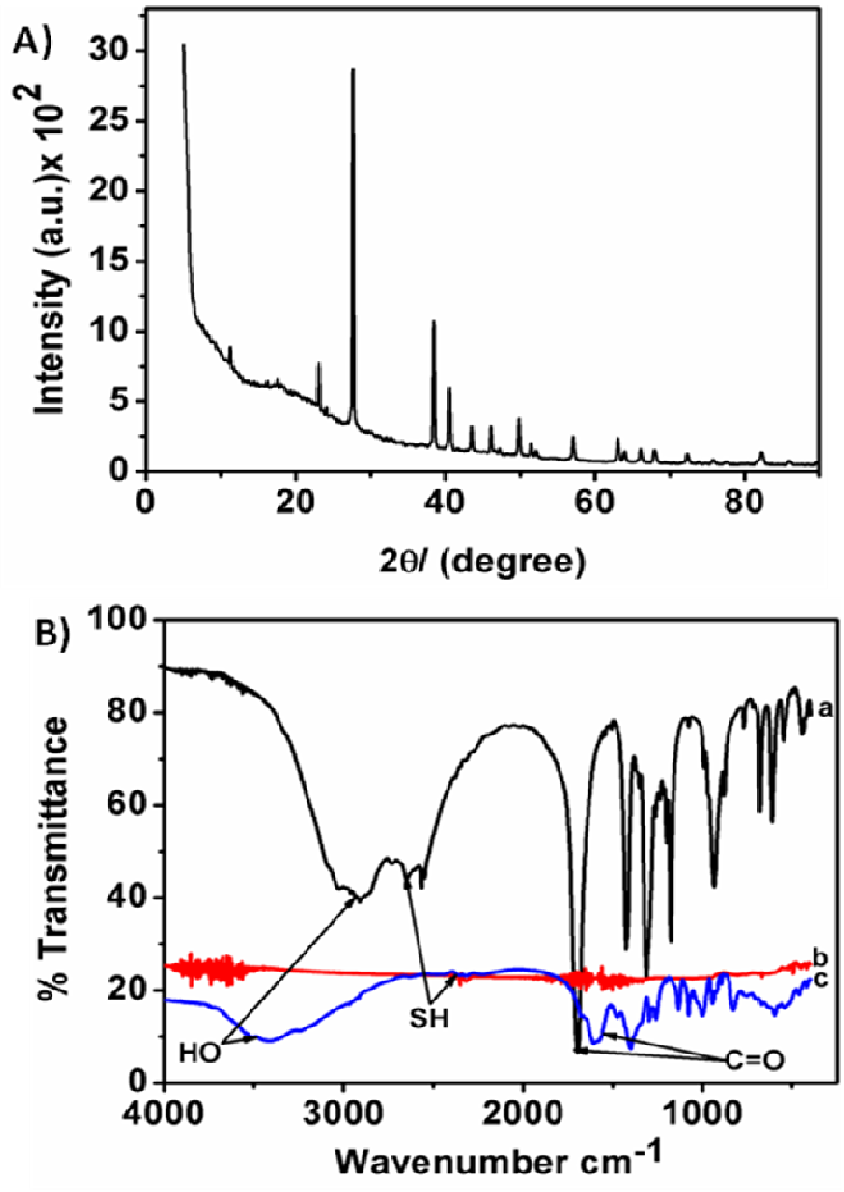

Fig. 2 (A) X-ray diffraction pattern of Ga_2Te_3 quantum dots. **(B)** FTIR spectra for (a) MPA, (b) Ga_2Te_3-MPA.

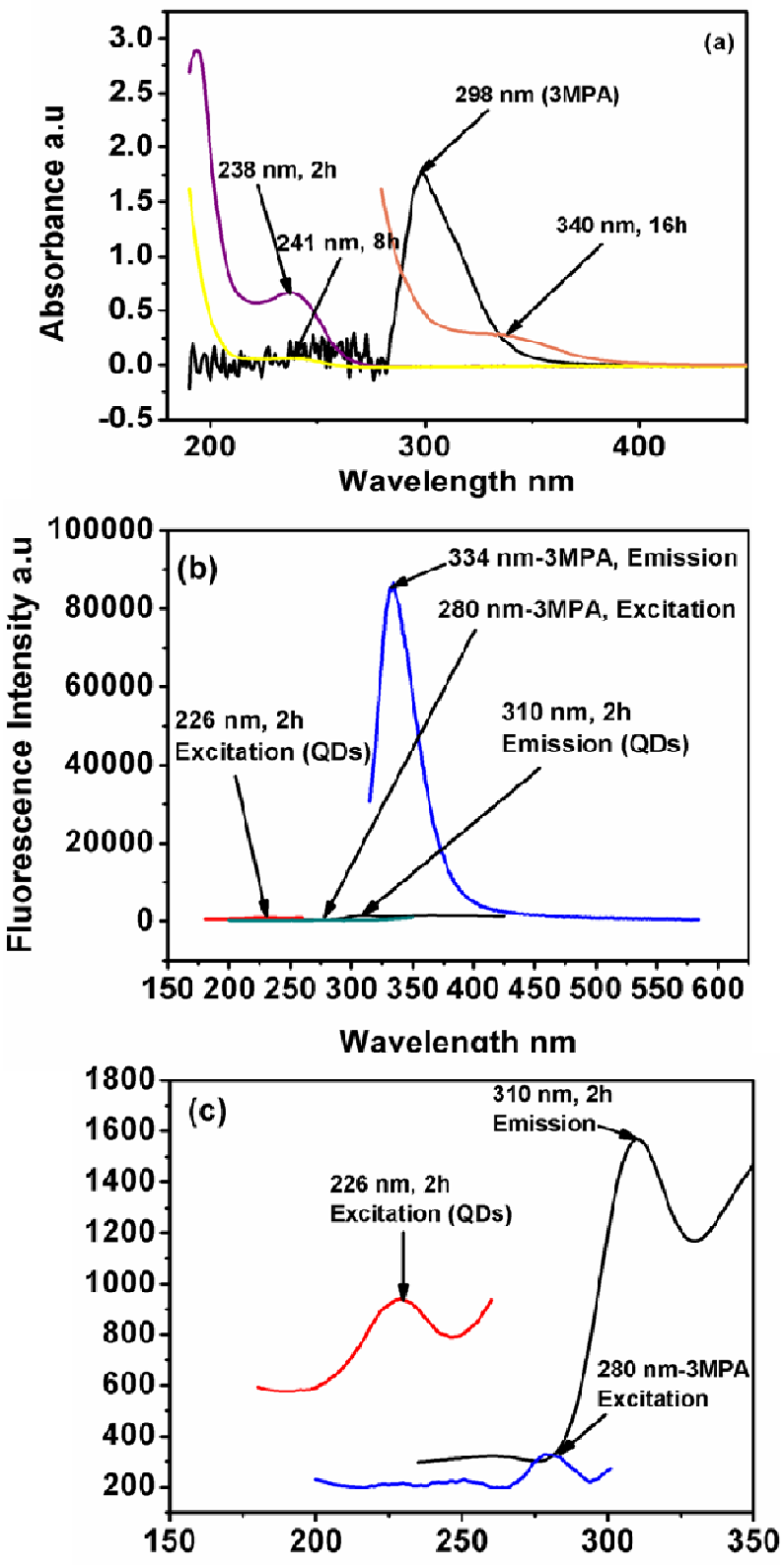

Fig 3 (a) UV-visible spectra of Ga_2Te_3-MPA in solution (before and during/after reflux). (b and c) Fluorescence spectra of Ga_2Te_3 showing both emission and excitation in solution.

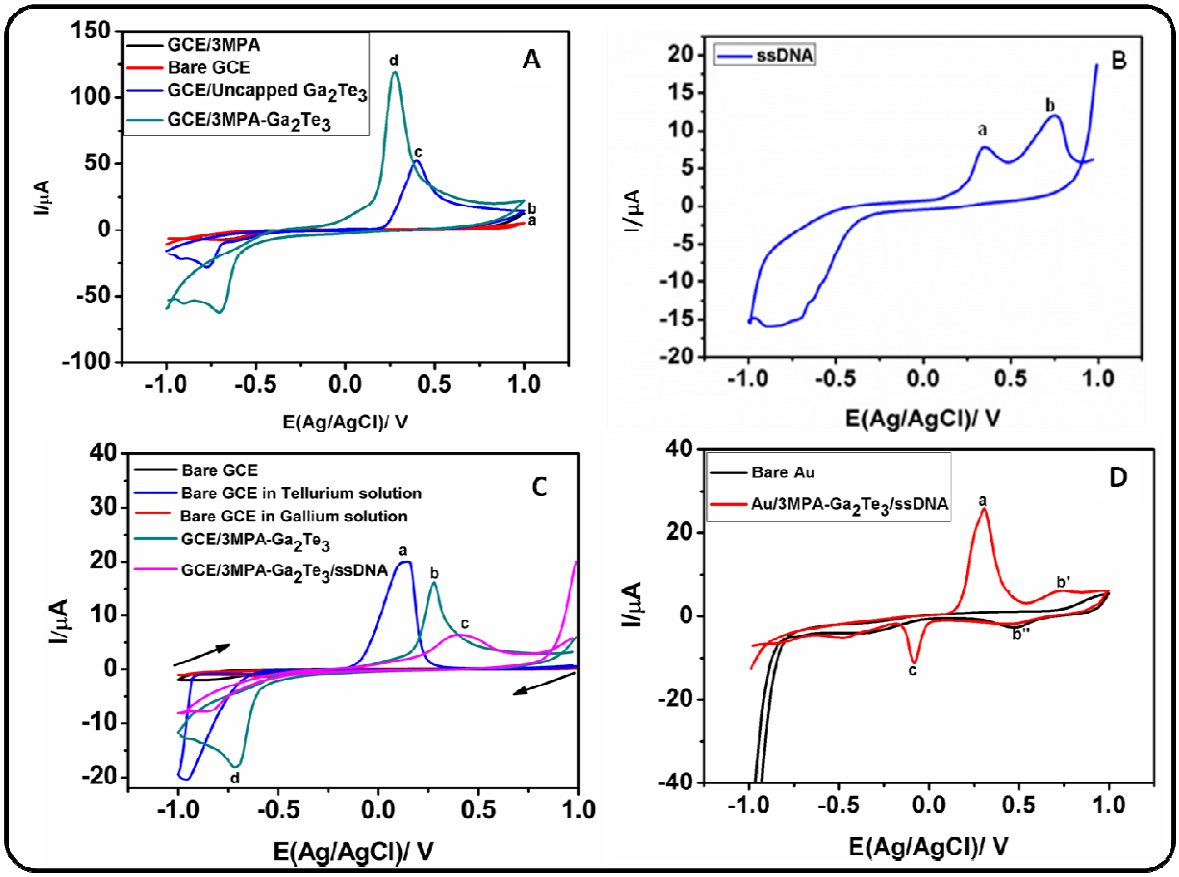

Fig 4. Cyclic voltammetric responses of electrode systems. (A) CVs of (a) bare GCE (b), MPA/GCE, (c) Ga_2Te_3/GCE and (d) Ga_2Te_3-MPA/GCE. (B) CV of ssDNA/GCE. (C) CVs of (a) Te/GCE, (b) Ga_2Te_3-MPA/GCE, (c) ssDNA/Ga_2Te_3-MPA/GCE and (d) bare GCE. (D) CVs of bare Au and ssDNA/Ga_2Te_3-MPA/Au. Experiments were performed in 0.1 M PBS (pH = 7.4) at 25 mV s^{-1}.

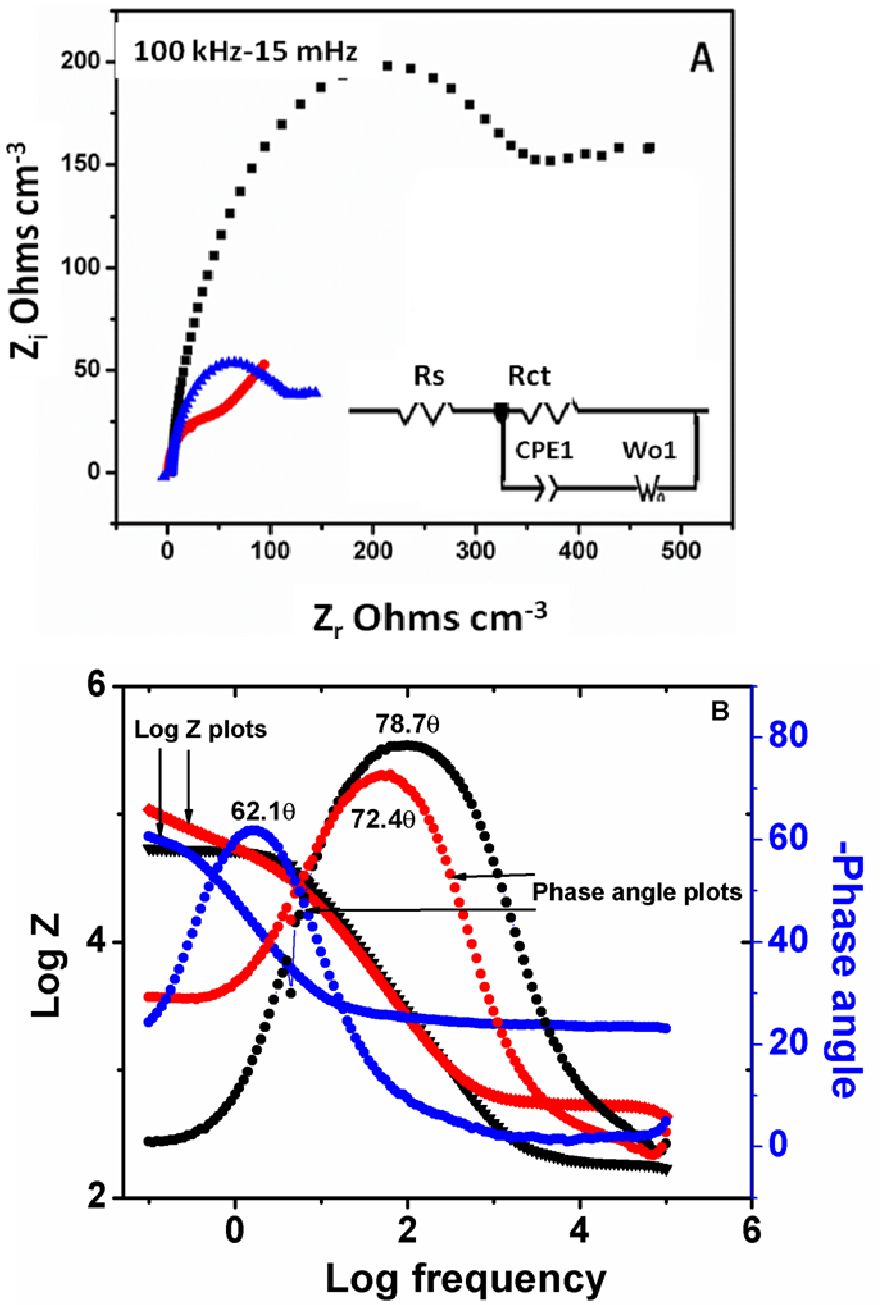

Fig 5. (A) Nyquist plots of bare Au (red symbols), Ga_2Te_3-MPA/Au (blue symbols) and ssDNA/Ga_2Te_3-MPA/Au (black symbols) electrodes in 0.1 M PBS (pH = 7.4). (B) The corresponding Bode plots of the EIS data in (A).

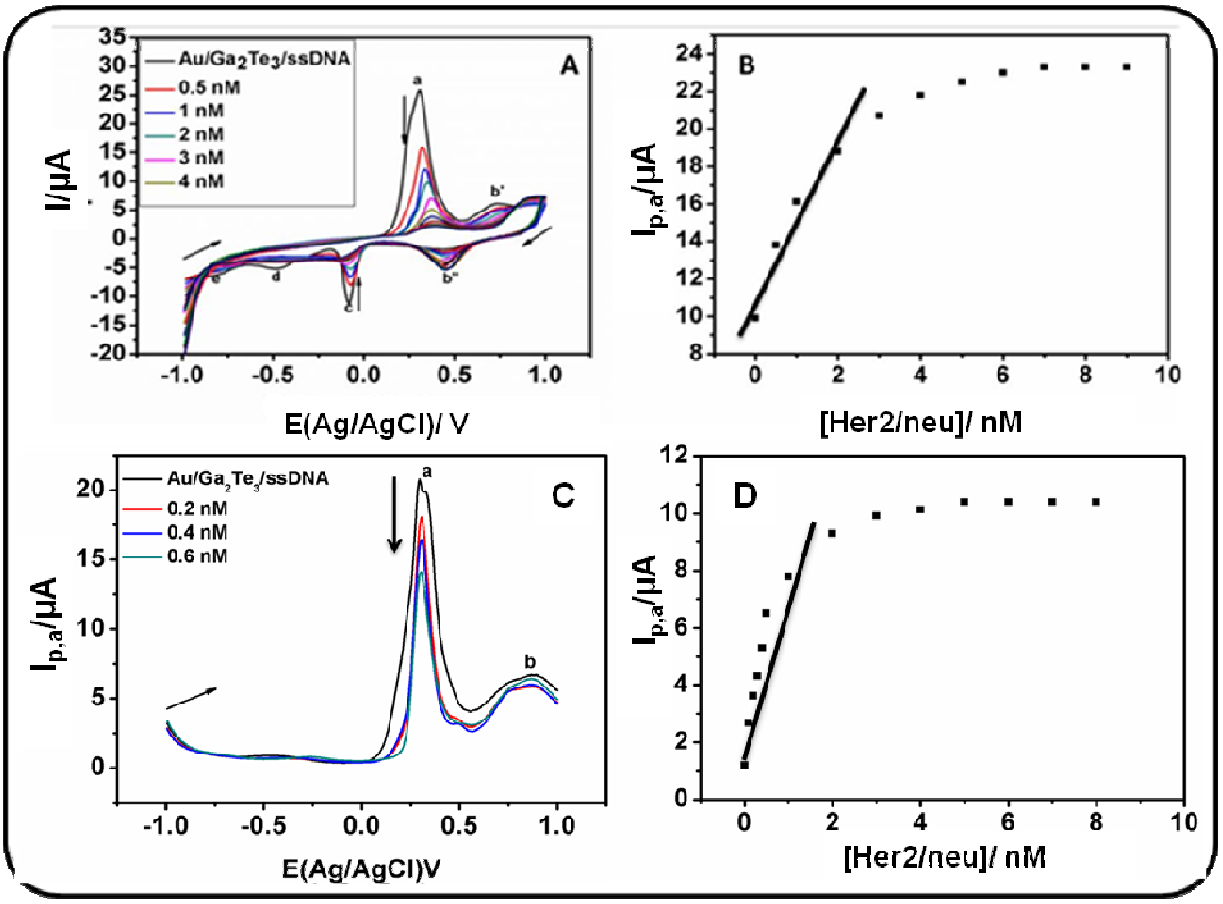

Fig 6. Genosensor (ssDNA/Ga_2Te_3-MPA/Au) responses to Her2 oncogene: (A) CVs, (B) calibration curve from CV data, (C) SWV and (D) calibration curve from SWV data. Typical concentrations of Her2 oncogene used are indicated in the graph. Experiments were performed in 0.1 M PBS (pH = 7.4) at 25 mV s^{-1}.

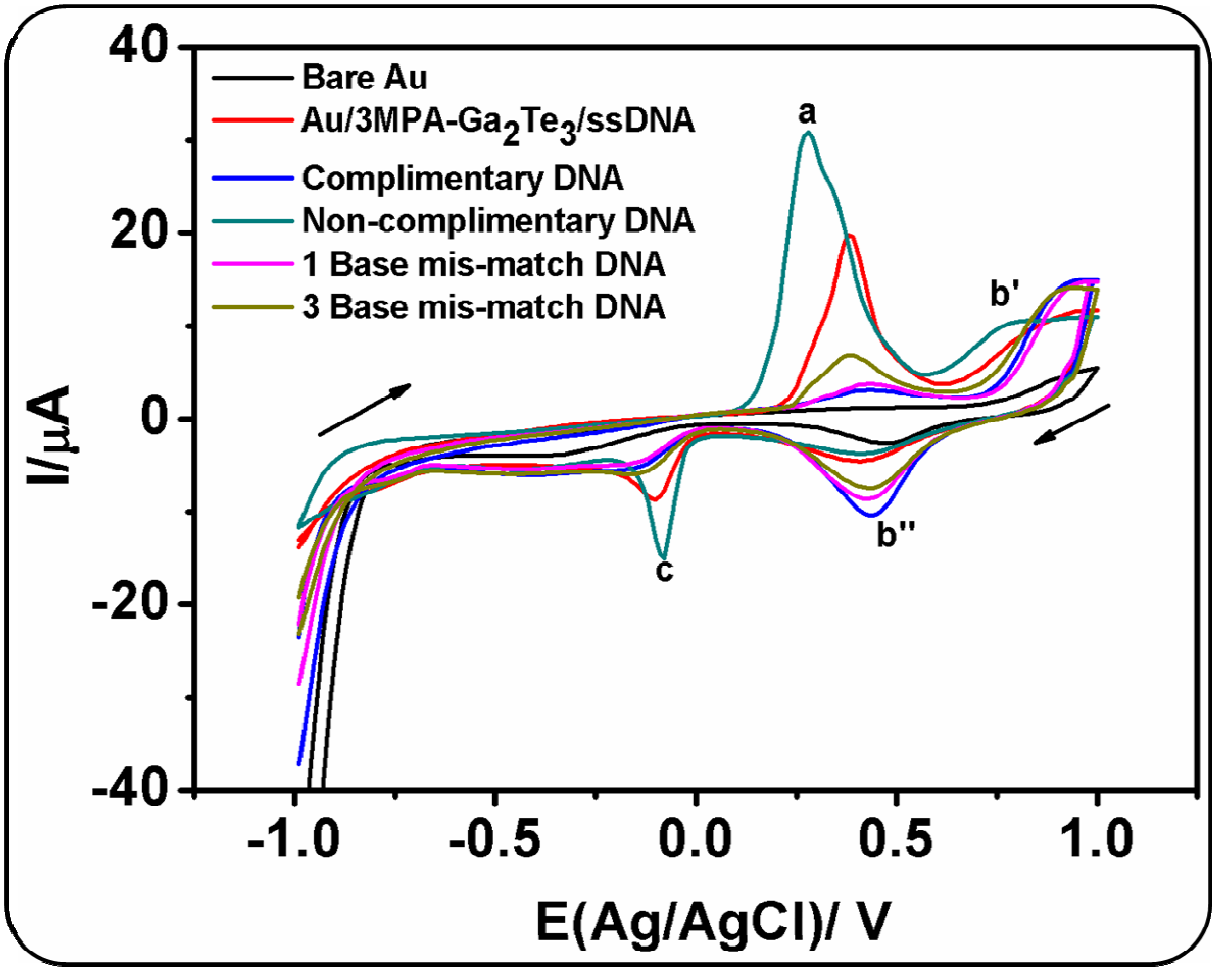

Fig. 7 Cross-reactivity of genosensor. Conditions are as in Fig. 6.

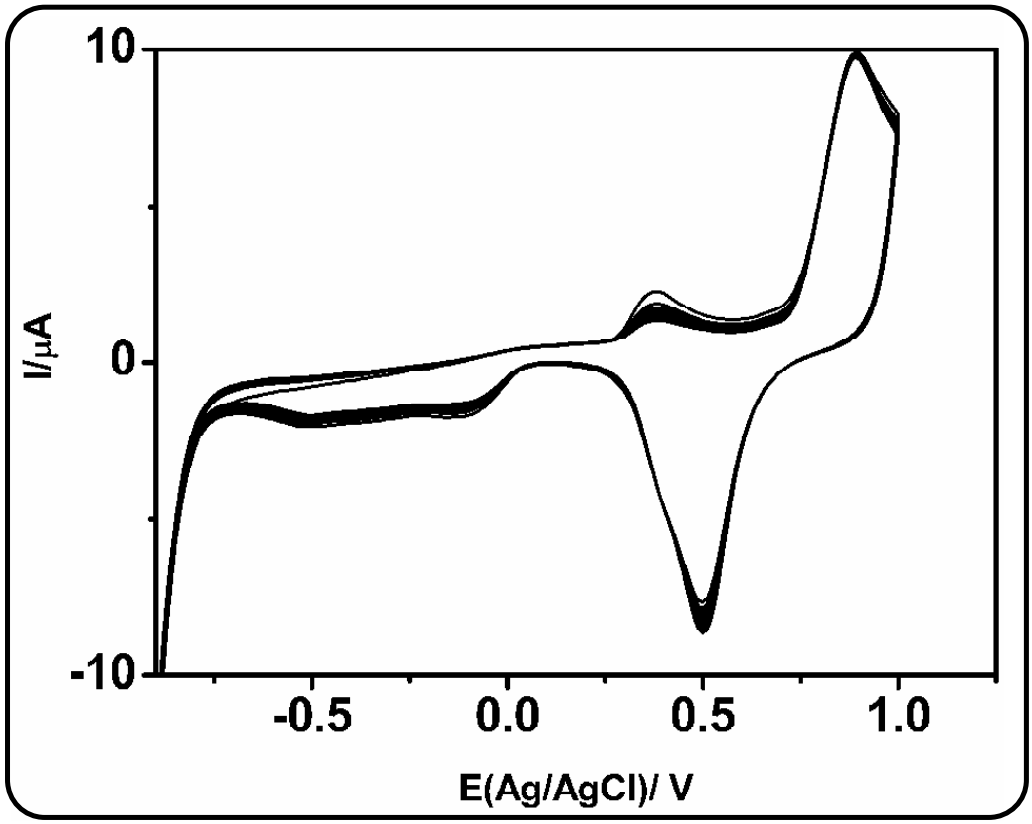

Fig. 8 Stability of genosensor. Conditions are as in Fig. 6.

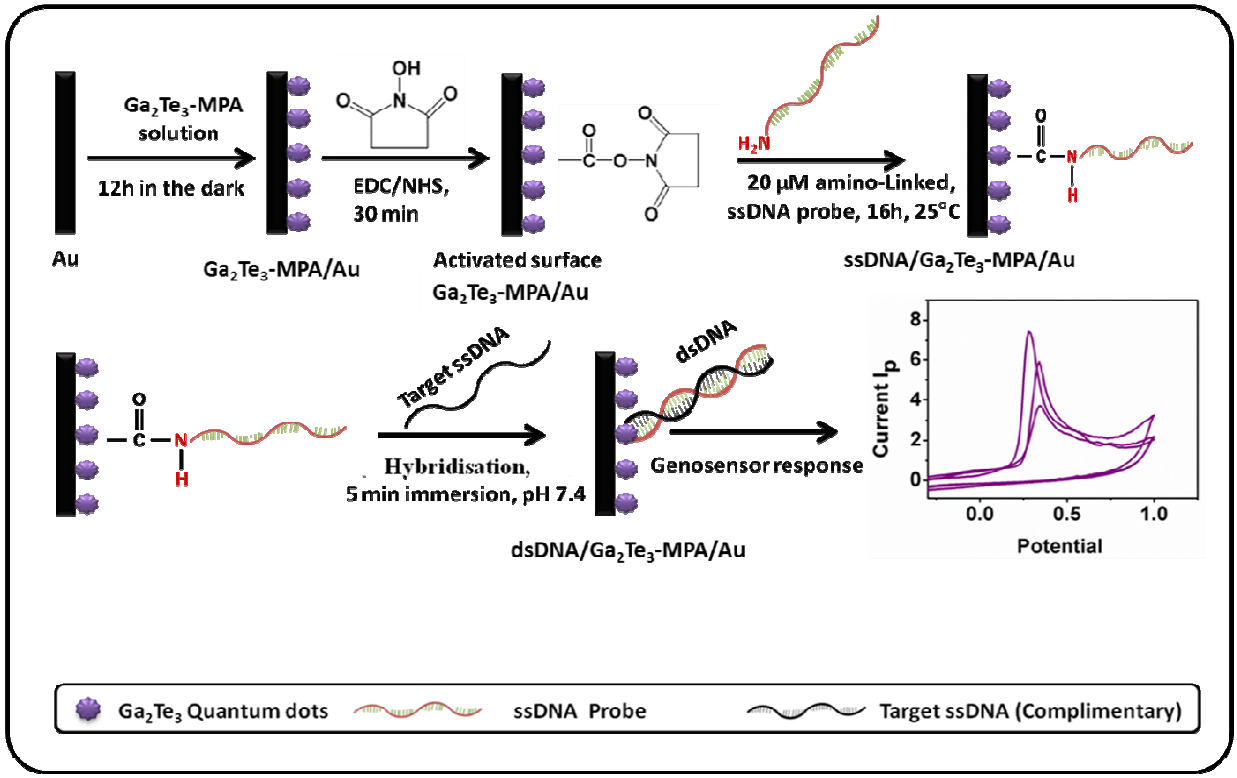

Scheme I. Preparation and response procedures of ssDNA/Ga_2Te_3-MPA/Au genosensor.

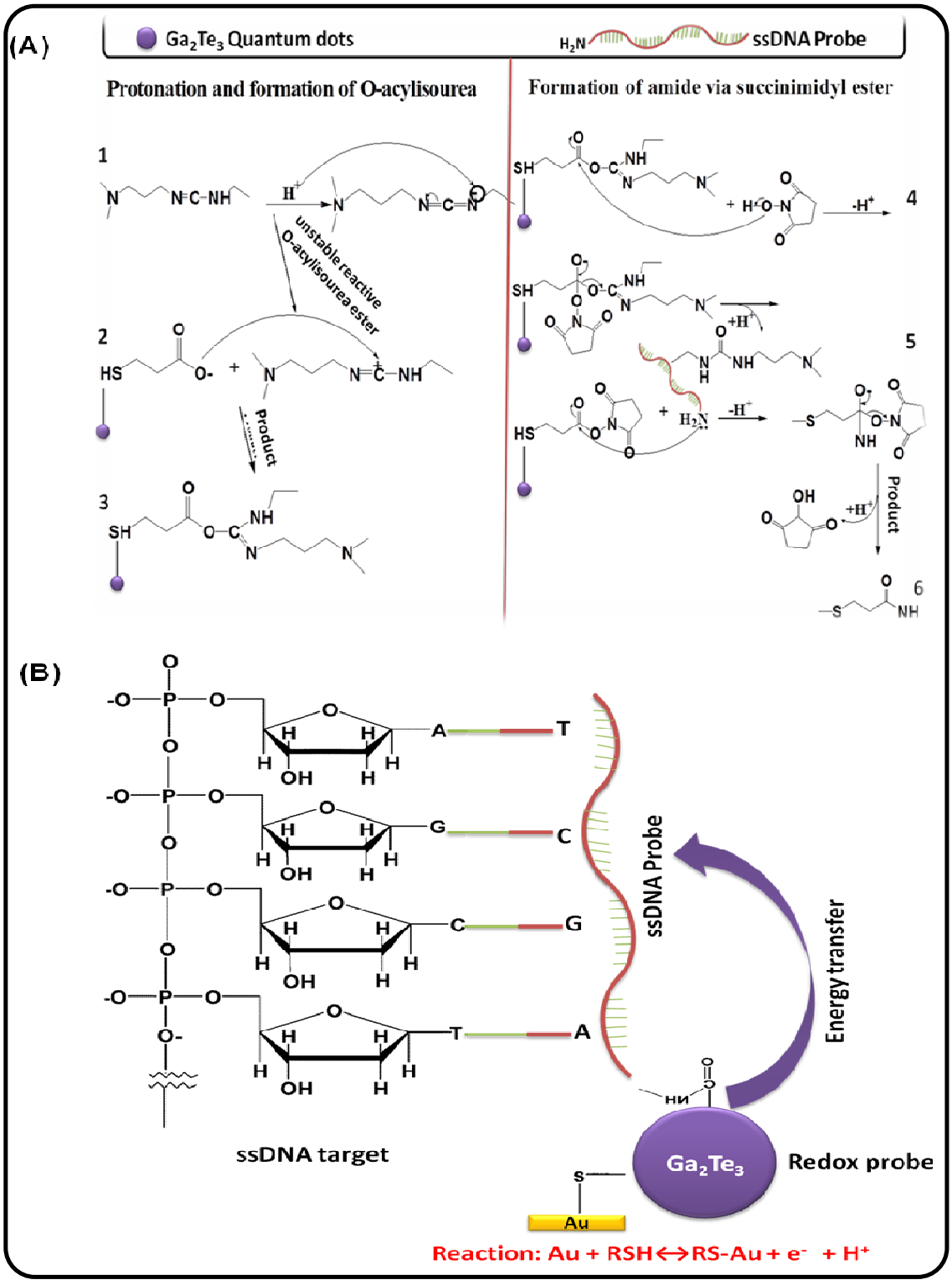

Scheme II: (A) The mechanism for the reaction of Ga_2Te_3-3MPA and probe-ssDNA with linkers (EDC/NHS). (B) The schematic diagram for the interaction of ssDNA/Ga_2Te_3-MPA/Au with target-ssDNA.